RSC Advances

ROYAL SOCIETY OF CHEMISTRY

www.rsc.org/advances

Solution blowing of activated carbon nanofibers for phenol adsorption

Xiaoxiao Tao, Guoqing Zhou, Xupin Zhuang*, Bowen Cheng*, Xiaojie Li, Hongjun Li

Key Laboratory of Advanced Textile Composite Materials of Ministry of Education, Tianjin Polytechnic University, Tianjin, P.R.China

Abstract

Activated carbon nanofiber (ACNF) with high surface area and excellent phenol adsorption capacity has been successfully fabricated by solution blowing of polyacrylontrile (PAN) into precursor nanofiber which was subsequently activated to ACNF via KOH activation process. The effects of impregnation ratio and activation temperature on the texture properties of ACNF were discussed. The texture properties were characterized by N_2 adsorption/desorption isotherm. ACNF showed high value of special surface area and pore volume (2921.263 m^2 g^{-1} and 2.714 cm^3 g^{-1}, respectively). The ACNF samples were used for phenol adsorption from aqueous solutions. Adsorption isotherms at 38 ºC were fitted with Langmuir and Freudlich models. The relationship between texture properties and phenol adsorption behavior was investigated. As a result, ACNF sample with large surface area, high micropore volume and pore size close and above to 0.43 nm showed the maximum phenol adsorption capacity of 251.6 mg g^{-1}.

1. Introduction

Over the last few decades, the occurrence of micropollutants in the aquatic environment has become a worldwide issue of increasing environmental concern.[1] Phenols are common micropollutants of high priority concerns since they are toxic even at low concentration and possible accumulate in the environment.[2, 3]

Currently, a variety of methods, such as solvent extraction, catalytic oxidation, adsorption, biodegradation, have been applied for the efficient removal of phenol from waste water.[3, 4] Among these methods, adsorption is regarded as the best for phenol removing due to its simple procedure and relatively low operation temperature.[5] A preferred adsorbent, activated carbon (AC), is widely used for the removal of phenol from the aqueous phase. Recently, various types of ACs have been developed for the aqueous phase removal of phenol, including waste materials-derived activated carbon, carbon nanotubes and activated carbon fibers (ACFs) et.al.[6-9] Activated carbon nanofiber (ACNF), which is perhaps the most attracting class of AC, is well known for its highly developed porosity, large specific surface area, and abundant functional groups, as well as excellent chemical and thermal stability. These unique characteristics make it a good candidate for gas adsorption[10, 11] and water treatment.[7, 12] Up to now, various types of AC have been intensive studied for phenol adsorption. Nonylphenol ethoxylate adsorption on ordered mesoporous carbon was enhanced with increasing special surface area of pores larger than 1.5 nm.[13] ACFs were used for effective adsorption of some substituted phenols.[8] ACNFs with specific surface area of 1075 m^2 g^{-1} also showed excellent phenol uptake of 377 mg g^{-1}. Therefore, microporous ACNF of high surface areas and large pore volumes with suitable pore sizes have great potential in phenol adsorption.

Generally, there are two approaches to produce ACNF: vapor growth[14] and electrospinning.[15] Unlike catalytic synthesis, electrospinning precursor solution followed by stabilization and activation is a straightforward and convenient route to make continuous ACNFs. Usually, the precursor nanofibers are fabricated by electrospinning polymer solution of polyacrylonitrile (PAN)[10] and phenolic resin[16]. The property of ACNF depends on the property of the precursor fiber as well as on the conditions of activation. PAN as a carbon precursor has been widely used to fabricate ACNF, but the main disadvantage of PAN-based ACNF is relatively low specific surface area.[16]

At present, few literature can be find about fabrication of high surface area ACNF (>2000 m^2 g^{-1}), especially for PAN-based ACNF. Most of electrospinning PAN-based ACNFs present special surface area ranging 200-1500 m^2 g^{-1}.[2, 10, 17-19] In this study, a new technology, solution blowing has been applied to fabricate PAN nanofiber, the precursor fiber. Unlike electrospinning using electrostatic force, this method uses high velocity airflow to attenuate polymer solution streams and collects the solidified nanofibers after solvent evaporation.[20, 21] The procedure has a fiber production rate several times higher than electrospinning and it is suitable for almost all kinds of polymer, especially for PAN, which cannot be molten.[20] In our previous works, SiC nanofibers[20], PVDF nanofiberous membrane[22] and ZnO/carbon composite nanofibers[21] were successfully fabricated with high yield and high quality. Thus, solution blowing is expected to be a more efficient, energy saving and safer method for mass production of nanofibers, which is superior to electrospinning.[22]

Similar to fabrication of electrospinning ACNF, ACNF can be prepared by solution blowing PAN followed by a three-step process: stabilization and impregnation and activation. In this paper, high surface area ACNF has been successfully prepared to develop effective adsorbent for phenol. The solution blowing ACNF webs could be one kind of hierarchical mesh adsorbent with large number of micropores and a few mesopores and macropores. Specific surface area and pore volume of ACNF can be tuned by controlling activation conditions.

2. Experimental

2.1 Chemicals

PAN filaments (Mw~90000) were from Toray Industries (China) Co., Ltd. They were washed and dried before used. Dimethylformamide (DMF) and phenol were from Tianjin Guangfu regent company.

2.2 Synthesis

Figure 1 showed the schematic of solution blowing apparatus，as our previous report.[20] The PAN/DMF solution was fed into a 0.5 mm inner diameter needle and injected at 10 mL $h^{-1}$with a peristaltic pump. Then the polymer solution was attenuated by high velocity airflow and sprayed into nanofibers which were collected on nylon nets. To evaporate DMF, the as-spun nanofiber web was dried at room temperature under vacuum overnight for subsequent treatment.

The PAN webs were stabilized under air atmosphere in a program controlled furnace and heated

from room temperature to 200 ºC at the rate of 5 ºC min^{-1}. The samples were held at 200 ºC for 30 min and then heated to 260 ºC at the rate of 2 ºC min^{-1} and held for 60 min. Then the stabilized nanofibers were infiltrated with 1M KOH for 12 h, at a series of impregnation ratio (KOH/PAN), and subsequently dried at 80 ºC till constant weight. Then the dried webs were heated from room temperature to activation temperature (600,700,800 ºC, respectively) at 5 ºC min^{-1} and held for 30 min under N_2 gas flow. Afterwards, the as-activated ACNF nonwoven fabric was rinsed with deionized water till the pH of filtrate was about 7. Finally, all the samples were dried under 110 ºC overnight. Table 1 shows the experiment conditions for preparing ACNF.

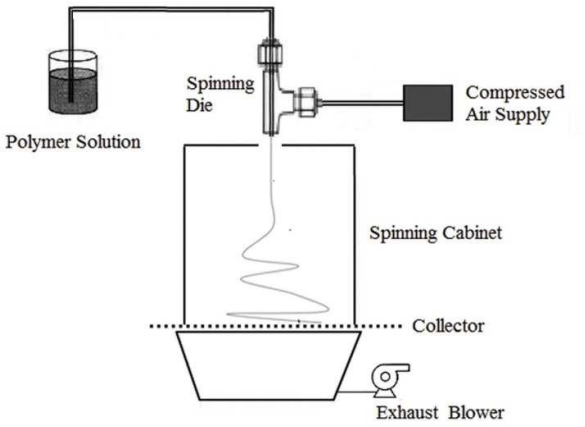

Figure 1 Schematic of the solution blowing spinning process

Table 1 Experiment conditions for preparing ACNF

Designation of sample	Impregnation ratio (KOH:PAN)	Activation temperature(ºC)	Activation time (min)
800I	1:3	800	30
800II	1:1	800	30
800III	3:1	800	30
700III	3:1	700	30
600III	3:1	600	30

2.3 Characterization

The microstructure and surface morphologies of stabilized nanofiber and activated carbon

nanofiber are observed by a field emission scanning electron microscope (FE-SEM) (S-4800, Hitachi co., Japan). The nitrogen adsorption/desorption, surface areas, pore volumes and pore size distribution were determined using a Quantachrome Nova 2020 e analyzer. The pore size distribution was calculated by the density functional theory (DFT). The ACNF samples were separately degassed at 200 ºC for 2h before measurement.

2.4 Adsorption of phenol

To investigate the adsorption capacity of ACNF, a batch of phenol adsorption test was conducted. Stock solutions were prepared by dissolving phenol in deionized water. For each time, 0.05 g of ACNF was placed in a conical flask, which contains 100ml phenol solution with different initial concentration. All conical flasks were placed in an air bath shaking table at 38 ºC for 48 h with a fixed speed of 120 rpm. Then the conical flasks were taken out and the solid liquid mixtures were filtrated to separate ACNF webs and solution. The phenol concentration was measured with a UV-VIS spectrophotometer (UV-1800，MAPADA instrument). The phenol adsorption capacity Qe (mg g^{-1}) was determined as the following formula

$$Q_e = \frac{(C_0 - C_e)V}{m} \quad (1)$$

where C_0 and C_e are the phenol concentration before and after 24 h batch adsorption respectively, V is the volume of aqueous solution containing phenol, and m is the mass of adsorbent.

Kinetic studies were performed following a similar procedure at 38 ºC. The initial phenol concentration was set as 300 mg L^{-1}. The uptake of the adsorbate at time t, Q_t (mg L^{-1}), was calculated by the following equation:.

$$Q_t = \frac{(C_0 - C_t)V}{m} \quad (2)$$

where C_t is the concentration of the adsorbate (mg L^{-1}) in solution at time t. All the experiments were done in triplicate with deviations below 5% in all cases; reported data represent the average values.

3. Results and discussion

For the fabrication process, the texture properties and phenol adsorption property of ACNF are related to a number of parameters. In this paper, the effects of the parameters including impregnation ratio and activating temperature on the texture properties are discussed, followed by

the relationship between texture properties and phenol adsorption.

3.1 Impregnation ratio

The weight ratio of KOH to PAN stabilized fiber web, namely impregnation ratio, has been found to be a crucial parameter in activation process.[23, 24] In this study, three level of impregnation ratio has been applied. Figure 2 a-d show the morphology of stabilized PAN nanofibers and ACNFs prepared with different impregnation ratio. It is observed that ACNFs presents a random arrangement. Activation treatment didn't change their morphology obviously. These activated fibers were continuous and uniform with the fiber diameter ranging 200-500 nm. The TEM images of 800III (Figure 2 d,e) clearly indicated that KOH activation process at high temperature lead to mesopores around 2 nm. The mesopores are highly unified and equally distributed. The N_2 adsorption isotherm of ACNF and the pore size distribution based on DFT model are present in Fig 3. The isotherm of 800I and 800II are similar and may be considered as type I of IUPAC classification, characterized of a sharp rise at low pressure (0-0.1) and a plateau at high pressure range, indicating the predominance of microporosity.[8] At relative pressure close to zero, the sharp vertical part of 800II is 405 $cm^3\ g^{-1}$ while the 800I is 262 $cm^3\ g^{-1}$, indicating the microporosity of 800II is higher than 800I. As the impregnation ratio increase from 1:3 to 1:1, the knee of isotherms became wider, followed by less broad plateau, indicating wider distribution of pore sizes. The isotherm of 800III shows no plateau at high relative pressures, meaning 800III may possess a kind of hierarchical pore size. As shown in Figure 3.b, pore size distribution became wide and complex with increasing impregnation ratio. The pore size distribution curve of 800I demonstrates that the distribution is quite narrow and pore size is centered at about 0.61nm. 800III exhibits a complex pore system consisting of not only the particular pores around 0.8nm but also a large number of other pores ranging from 1.8 to 4 nm. These sequential mesopore channels lead to reversible N_2 adsorption and desorption. The textural properties, including BET, total pore volume, micropore volume and mesopore volume are list in Table 2.

Inspection of Figure 3.b. and Table 2 show the following: (i) the BET surface area increased considerably to 2662 $m^2\ g^{-1}$ and micropore volume multiplied when the impregnation ratio increased from 1:3 to 1:1. Because increasing impregnation ratio is associated with a progressive development in micropore structure when the content of KOH is not sufficient. (ii) The increase of impregnation ratio from 1:1 to 3:1 resulted in a little change in BET and micropore volume, but a

remarkable improved mesopore volume. These were generally attributed to further activation, which broadened part of micropores into mesopores and expanded mesopores sizes.[24] It is well-known that the removal of the chemicals left in the carbonized sample by washing will increase the porosity in the carbon structure, and the distribution of these chemicals in the precursor prior to carbonization governs the pore size distribution in the final products.[25] (iii) In first stage, KOH activation created a large amount of micropores up to micropore volume of 1.38 cm^3 g^{-1}. Next, activation kept generating micropores and expanded some of them to mesopores. Therefore, pore structure of ACNF can be manipulated by controlling the content of KOH, especially for micropores. Severer activation conditions, namely high impregnation ratio here introduced mixed micropores and mesopores, which would decrease the homogeneity. In this paper, ACNF samples with three different pore structures and surface area have been fabricated, namely 800I with micropore only, 800II with majority of micropore and a few mesopores, 800III with nearly half micropores and half mesopores.

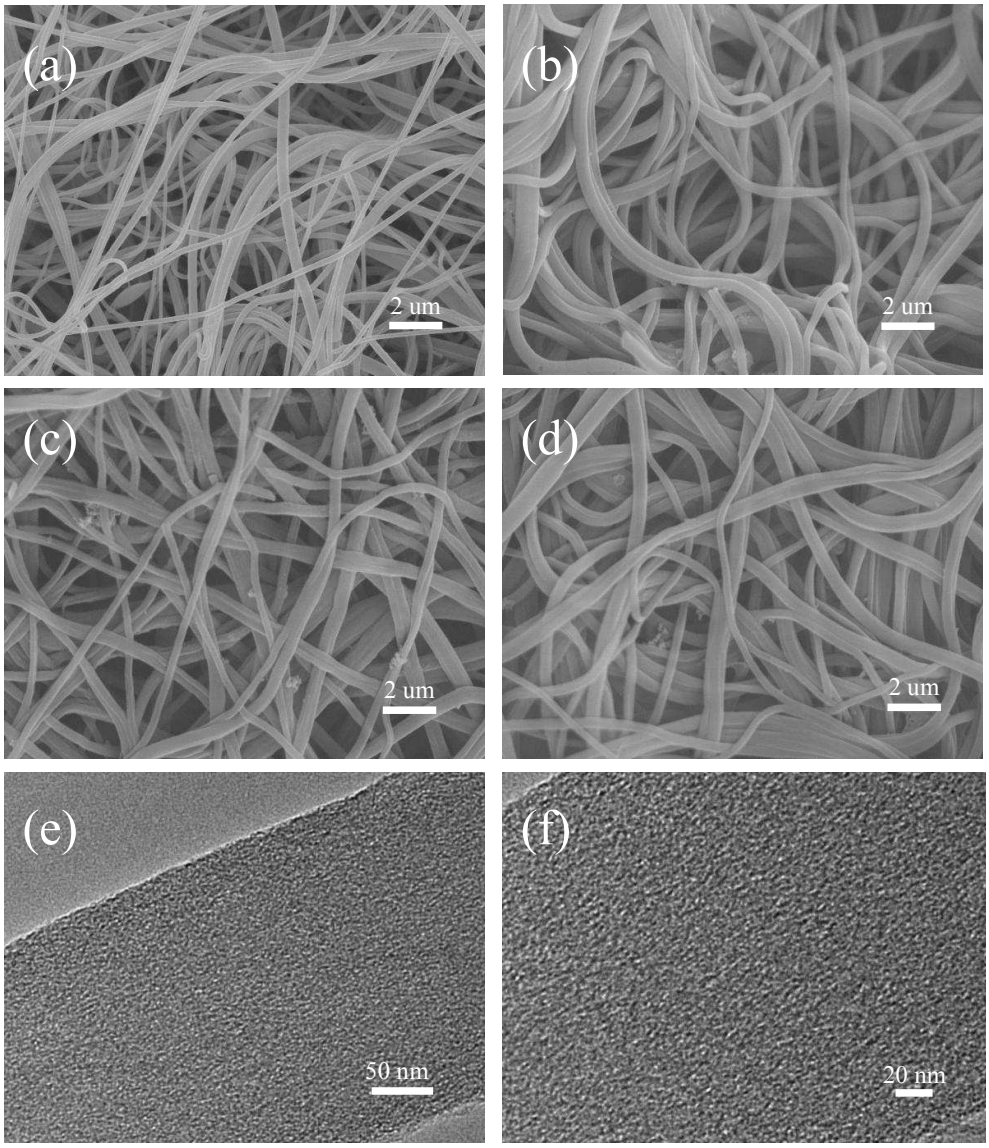

Figure 2 SEM images of (a) stabilized PAN nanofiber, (b) 800I, (c) 800II, (d) 800III, (e) TEM image of 800III, (f) magnification of e

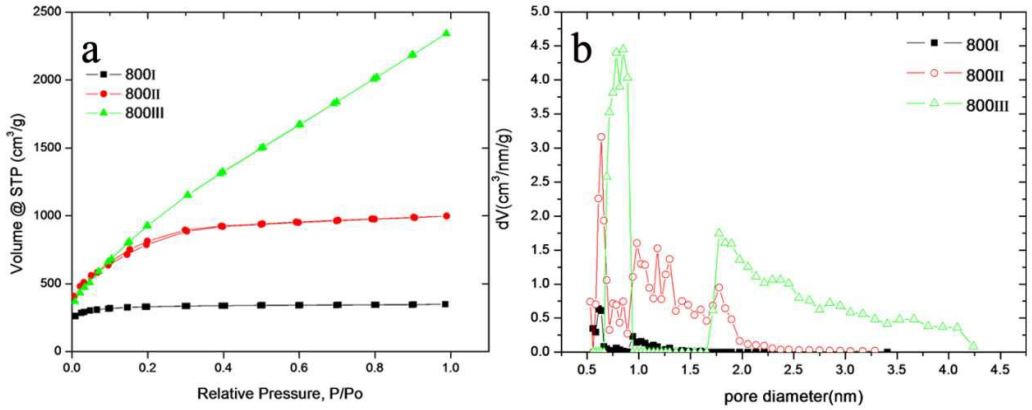

Figure 3 (a) N_2 adsorption/desorption isotherms of 800I and 800II and 800III, (b) Pore size distribution of 800I and 800II and 800III calculated by DFT

Table 2 Texture property of ACNF fabricated with different impregnation ratio

Sample	BET(m^2 g^{-1})	Vtotal(cm^3 g^{-1})	Vmicro(cm^3 g^{-1})	Vmeso(cm^3 g^{-1})	Daverage(nm)
800I	1260.018	0.504	0.504	0	0.610
800II	2662	1.441	1.3873	0.0637	0.6365
800III	2921.263	2.714	1.3171	1.3966	0.848

3.2 Activating temperature

N_2 adsorption/desorption isotherms of 600III and 700III and 800III and pore size distribution of the three samples calculated by DFT are presented in Figure 4. It is evident that the isotherm of 600III and 700III are type I isotherm in Figure 4.a. These three ACNFs adsorbed nitrogen at low relative pressure, which indicated that the samples had well developed micropores. As activation temperature rise from 600 to 800 ºC, the volume at low relative pressure changed a little, but the plateau at high relative pressure narrowed down in sequence. The results were consistent with pore size distribution from Figure 4 b. The micropores of the three samples were fully developed, while the size of pores became larger. It can be observed that the amount of micropores stayed the same but mesopores increased significantly. In other word, on the condition that impregnation ratio was as high as 3:1, the mesopore growth was depending on activating temperature. Higher activating temperature resulted in larger pore size. Table 3 demonstrated the texture properties of 600III~800III. The increase of activation temperature from 600 to 800 ºC was associated with a progressive development in mesopore volume and the total pore volume and special surface area, while micorpore volume improved slightly from 1.0835 cm^3 g^{-1} to 1.3171 cm^3 g^{-1}. Hence, under a fixed impregnation ratio of 3:1, the mesopore structure of ACNF can be tunable by changing

activation temperature. In this work, high surface area ACNFs above 2300 m^2 g^{-1} have been successfully prepared, with tunable mesopore volume.

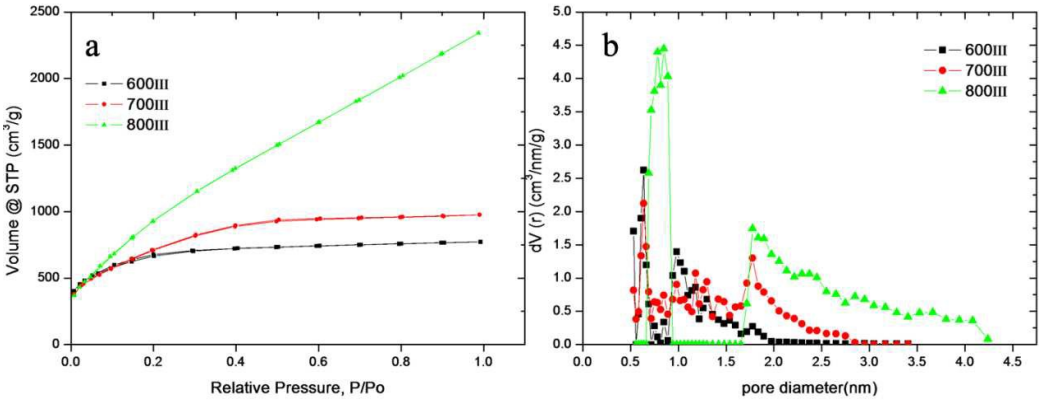

Figure 4 (a) N_2 adsorption/desorption isotherms of 600III and 700III and 800III, (b) Pore size distribution of 600III and 700III and 800III

Table 3 Texture property of ACNF fabricated with different activation temperature

Sample	BET(m^2 g^{-1})	Vtotal(cm^3 g^{-1})	Vmicro(cm^3 g^{-1})	Vmeso(cm^3 g^{-1})	Daverage(nm)
600III	2315.823	1.113	1.0835	0.029	0.636
700III	2583	1.437	1.225	0.212	1.437
800III	2921.263	2.714	1.3171	1.3966	0.848

3.3 Relationship between texture property and phenol adsorption

3.3.1 Adsorption isotherms

Besides pore size and surface area, the structural match between adsorbent and adsorbate also affects the adsorption amount.[26] The molecules with a suitable size would be adsorbed more favorably since they have more contact sites with carbon surface.[8] It is important that the available pore size is larger than the cross section distance of adsorbate, since adsorption is possible only in those pores which can be entered by adsorbate molecules. The smallest cross-section distance for phenol in aqueous solution is 0.43 nm[27] and promising pore size of adsorbent should be slightly larger but closed to 0.43 nm. [2]The ACNFs have five different types of pore size distribution and pore volume as Table 3 and Table 4 show. The micropore volume follows the order: 800III> 800II> 700III> 600III> 800I. Among them, 800I, 800II and 600I have micropore size that closer to cross-section distance of phenol (0.43nm), while 800III and 700III show larger pore size. Compared all ACNFs, 800I has the most narrow micropore size distribution, the order followed by

600III, 800II, 700III, 800III.

Adsorption isotherm is important to describe the interaction between solute and adsorbents. Herein, two widely used phenomenological equations were applied to fit the equilibrium data, namely Langmuir and Freudlich equations.

Langmuir isotherm model assumes that a maximum limiting uptake exists, corresponding to a saturated monolayer of adsorbate molecules at the adsorbent surface and adsorption process will only take place at specific homogenous site.[28] The Langmuir equation is given by:

$$Q_e = \frac{Q_0 \times K_L \times c_e}{1 + K_L \times c_e} \quad (2)$$

where Qe (mg g^{-1}) is the amount of adsorbed phenol, and Ce (mg L^{-1}) is the residual concentration of solution at equilibrium. Q_0 is the maximal adsorption capacity, and K_L is a constant related to the affinity of binding sites.

Freudlich isotherm model is an empirical equation assuming that adsorption occurs on a heterogeneous surface through a multilayer adsorption mechanism, and the adsorbed amount increases with the concentration.[29] Freudlich equation is given by

$$Q_e = K_F \times c_e^{1/n} \quad (3)$$

where K_F is a constant represents adsorption capacity (mg g^{-1}·(mg L^{-1})^n), n is the empirical parameter representing the energetic heterogeneity of the adsorption sites.

The adsorption isotherms of phenol on ACNFs at 38 ºC were presented in Figure 5 (a)-(e): (a) 800I, (b) 800II, (c) 800III, (d) 700III, (e) 600III. All of them were fitted by the three models cited above. All curves rise quickly at low concentration and gradually approach a plateau at high concentration. Compared to others, 800I, 800II and 600III demonstrate more intense adsorption capacity at low concentration, which should attribute to their micropore size around 0.6nm, closer enough to the cross-section distance of phenol. When it comes to high concentration, 600III presents the highest adsorption capacity, followed by 800I and 800II.

The result fitting parameters were calculated and summarized in Table 4. The values of Q_0 are found to vary between 119 and 251 mg g^{-1} for 800III and 600III, respectively. The goodness of the fit is characterized by the value of R^2. The Freundlich equations fit all the fifth samples well with coefficients (R^2) in the range of 0.96~0.99 (Table 4), while Langmuir model is usable for 800I,

800II, 600III and 700III but not for 800III (R_L=0.89). Therefore, the Freudlich model is reasonably applied in all cases. This phenomenon illustrated that 800III has heterogeneous adsorbent surface more than homogeneous and other ACNFs possess both mono and heterolayers.[28]

Though the Langmuir equation is not the best to describe the isotherms, the parameter Q_0 is often considered as the adsorption capacity. The comparison of different ACNFs shows the following adsorption order: 600III>800I, 700III, 800II>800III. The similar sequence can be found from the value of K_F. Adsorption is considered as satisfactory when the Freudlich constant n takes values within the range 1-10, meanwhile indicating favorable adsorption of phenol.[29] Although 800I has the most narrow micropore distribution and proper pore size, its adsorption ability at high concentration was limited by its relatively low pore volume. In general, from the aspect of micropore volume and pore size distribution, 600III shows the best adsorption behavior at both low and high concentration. In summary, the texture property of ACNF controlled the adsorption behavior. As for phenol adsorption, idea adsorbent should have high micropore volume, narrow micropore distribution, pore size above and close to 0.43 nm. Here, the 600III meet with all the above features perfectly, indicating 600III can be excellent adsorbent for phenol. The phenol adsorption capacity of 600III is 251.6 mg g^{-1}, which is higher than ACF (200 mg g^{-1})[7] and aminated AC (243.47 mg g^{-1}).[30]. Although ACNF became brittle to handle after activation, compared with AC, ACNF still maintained fiber web form and is facile for application.

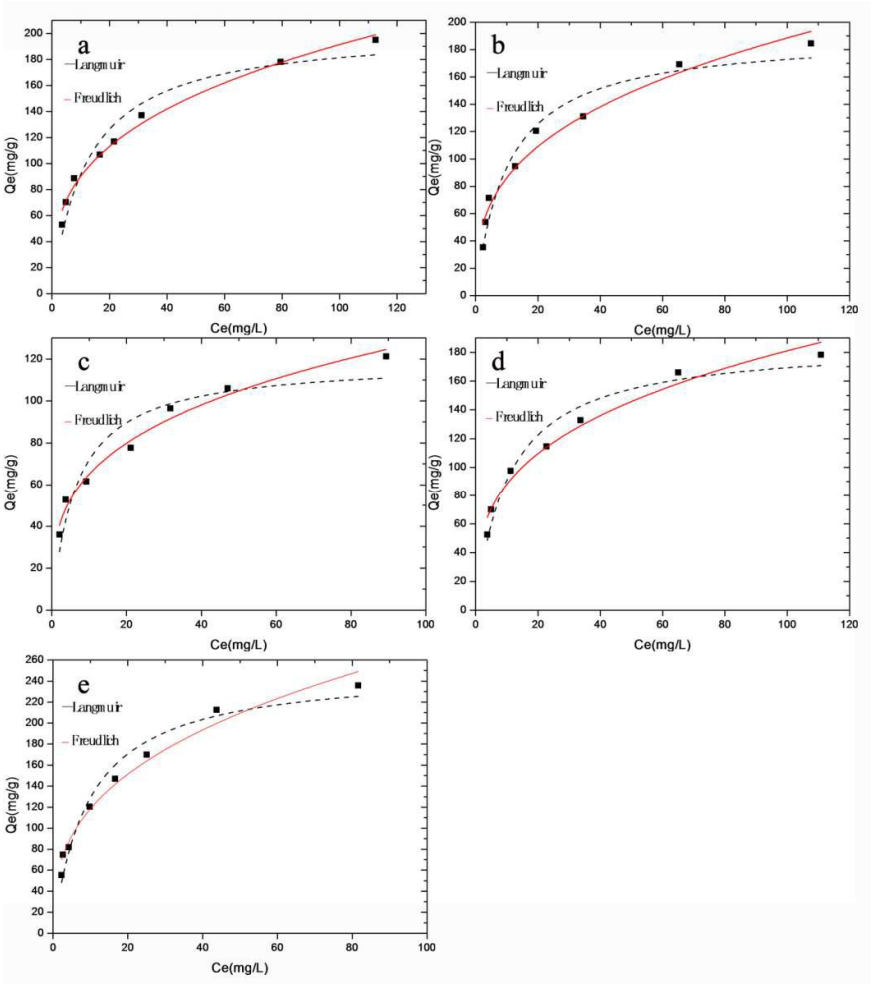

Figure 5 Phenol adsorption isotherms of (a) 800I (b) 800II (c) 800III (d) 700III (e) 600III

Table 4 Isotherms constants for adsorption of phenol on ACNF at 38 ºC

Sample	Langmuir			Freudlich		
	K_L (L mg^{-1})	Q_0 (mg g^{-1})	R^2	n	K_F (mg g-1)·(mg L^{-1})^n	R^2
800I	0.082	203.37	0.95	3.06	42.48	0.99
800II	0.097	190.65	0.95	2.94	39.44	0.96
800III	0.153	119.01	0.89	3.38	32.94	0.98
700III	0.095	187.072	0.96	3.2	42.9	0.97
600III	0.106	251.60	0.96	2.83	52.51	0.98

3.3.2 Kinetics studies

In order to further learn the adsorption behavior of these ACNF samples, kinetics of two typical samples (600III and 800III) were investigated .Figure 6 shows the plots of adsorption amount versus time. As can be seen, the ACNF shows fast adsorption behavior and curves reached rapidly to a plateau. It just takes 30 min to reach 90% of the total amount. Due to the open pore structure of ACNF, the diffusion resistance is reduced to a large extent.[31] Besides, the nonwoven fiberous form of ACNF also contributes to the fast adsorption kinetics, which helps to reduce the external mass transfer resistance.[8, 32]

In the present work, the pseudo-first-order, pseudo-second-order models were used to investigate the adsorption of phenol.

The pseudo-first-order model can be expressed as:

$$\ln(Q_e - Q_t) = \ln Q_e - k_1 t \quad (4)$$

where k_1 is the first-order rate constant, Q_e and Q_t (mg g^{-1})are the amount of phenol adsorbed at equilibrium and at any time, respectively.

The pseudo-second-order model can be expressed as:

$$\frac{t}{Q_t} = \frac{1}{k_2 Q_e^{\,2}} + \frac{t}{Q_e} \quad (5)$$

where k_2 is the second-order model constant.

The fitting constants of two models are listed in Table 5. The pseudo-first-order model gives poor fitting with low R^2 values and notable deviations between the experimental and theoretical uptakes. The pseudo-second-order model fits the data well for the adsorption of both 600III and 800III, the R^2 values are close to unity and the experimental and theoretical uptakes are in good agreement. Recently, some studies[8, 33] stated that the pseudo-second-order was suitable for the adsorption of lower molecular weight adsorbates on smaller adsorbent particles, which could explain for its applicability in this study. Thus, it can be assumed that the pseudo-second-order adsorption mechanism was predominant in the adsorption of phenol on ACNF.

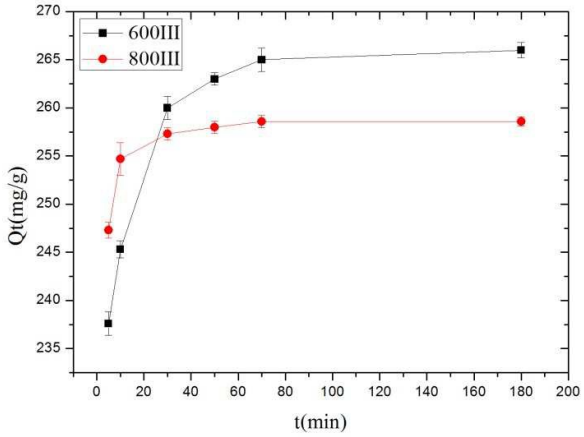

Figure 6 Adsorption kinetics of phenol on ACNF: 38 ºC, initial concentration 300 mg L^{-1}

Table 5 Pseudo-first-order and pseudo-second-order constants for the adsorption of phenol on ACNF at 38 ºC

Samples	Q_{exp} [a] (mg g^{-1})	Pseudo-first order			Pseudo-second order		
		Q_e (mg g^{-1})	k_1 (min^{-1})	R^2	Q_e (mg g^{-1})	k_2 (g mg^{-1} min)	R^2
600III	266	260.9	0.46	0.6	266.1	0.0057	0.95
800III	258.6	257.6	0.64	0.89	259.37	0.017	0.97

[a] Experimental uptakes, obtained after 48 h.

4. Conclusions

To sum up, a combined process of novel spinning and KOH activation is presented to fabricate ACNF for the phenol adsorption. The distinct ratio of impregnation and activation temperature influenced the texture property of ACNF, which lead to different adsorption behavior of phenol. The adsorption capability turned out to be a combined effect of special surface area, pore volume and pore size distribution. All the synthesized ACNF samples show excellent phenol adsorption capacity. The maximum surface area and pore volume are 2921.263m^2 g^{-1} and 2.714cm^3 g^{-1} for 800III, respectively, which are larger than most of activated carbon nanofiber. The N_2 adsorption/desorption isotherms showed that high impregnation ratio (KOH: PAN= 3:1) led to high surface area. DFT and pore size distribution results confirmed that activation temperature has a significant effect on mesopore volume. The phenol adsorption capacity displays a good correlation between micropore volume and pore size distribution of ACNF samples using Langmuir and Freudlich model. The maximum phenol adsorption capacity is 251mg g^{-1} at 38 ºC.

In kinetic studies, ACNF show high adsorption rate due to their open pore structure. The pseudo-second-order model gives satisfactory fitting. The fabricated ACNF could be considered as a good candidate for elimination of micropollutants from wastewater. This study provides a facile route for the synthesis of ACNFs.

Acknowledgements

The author would like to thank National Natural Science Foundation of China (51103104 and 51173131), Tianjin Natural Science Foundation (13JCZDJC32600) and Technology program of Tianjin Municipal Education Commission (20130324) for their financial support.

References

1. Y. L. Luo, W. S. Guo, H. H. Ngo, L. D. Nghiem, F. I. Hai, J. Zhang, S. Liang and X. C. C. Wang, *Sci. Total Environ.*, 2014, **473**, 619-641.
2. Y. Yang, Z. Mei-Hua, X. Gang and J. Zheng-Xiong, *Journal of Porous Materials*, 2010, **18**, 379-387.
3. S. H. Lin and R. S. Juang, *Journal of environmental management*, 2009, **90**, 1336-1349.
4. C. Y. Su, Y. F. Tong, M. Y. Zhang, Y. Zhang and C. L. Shao, *RSC Adv.*, 2013, **3**, 7503-7512.
5. E. Haque, J. W. Jun, S. N. Talapaneni, A. Vinu and S. H. Jhung, *J. Mater. Chem.*, 2010, **20**, 10801.
6. V. K. Gupta, A. Nayak, S. Agarwal and I. Tyagi, *Journal of colloid and interface science*, 2014, **417**, 420-430.
7. A. Chakraborty, D. Deva, A. Sharma and N. Verma, *Journal of colloid and interface science*, 2011, **359**, 228-239.
8. Q.-S. Liu, T. Zheng, P. Wang, J.-P. Jiang and N. Li, *Chemical Engineering Journal*, 2010, **157**, 348-356.
9. J. M. Dias, M. C. Alvim-Ferraz, M. F. Almeida, J. Rivera-Utrilla and M. Sanchez-Polo, *Journal of environmental management*, 2007, **85**, 833-846.
10. K. J. Lee, N. Shiratori, G. H. Lee, J. Miyawaki, I. Mochida, S.-H. Yoon and J. Jang, *Carbon*, 2010, **48**, 4248-4255.
11. G. Y. Oh, Y. W. Ju, M. Y. Kim, H. R. Jung, H. J. Kim and W. J. Lee, *Sci. Total Environ.*, 2008, **393**, 341-347.
12. M. Teng, J. Qiao, F. Li and P. K. Bera, *Carbon*, 2012, **50**, 2877-2886.
13. X. Yuan, W. Xing, S. P. Zhuo, W. J. Si, X. L. Gao, Z. H. Han and Z. F. Yan, *Journal of colloid and interface science*, 2008, **322**, 558-565.
14. R. R. Bacsa, C. Laurent, A. Peigney, W. S. Bacsa, T. Vaugien and A. Rousset, *Chem. Phys. Lett.*, 2000, **323**, 566-571.
15. L. F. Zhang, A. Aboagye, A. Kelkar, C. L. Lai and H. Fong, *J. Mater. Sci.*, 2014, **49**, 463-480.
16. Y. Bai, Z.-H. Huang and F. Kang, *Carbon*, 2014, **66**, 705-712.
17. S. S. Manickam, U. Karra, L. Huang, N.-N. Bui, B. Li and J. R. McCutcheon, *Carbon*, 2013, **53**, 19-28.
18. C.-I. Su, Y.-X. Huang, J.-W. Wong, C.-H. Lu and C.-M. Wang, *Fibers and Polymers*, 2012, **13**, 436-442.
19. G. Wang, C. Pan, L. Wang, Q. Dong, C. Yu, Z. Zhao and J. Qiu, *Electrochimica Acta*, 2012, **69**, 65-70.
20. G. Yan, X. Zhuang, X. Tao and B. Cheng, *Science of Advanced Materials*, 2013, **5**, 209-215.
21. S. Shi, X. Zhuang, B. Cheng and X. Wang, *J. Mater. Chem. A*, 2013, **1**, 13779.
22. X. Zhuang, L. Shi, K. Jia, B. Cheng and W. Kang, *Journal of Membrane Science*, 2013, **429**, 66-70.
23. S.-H. Yoon, S. Lim, Y. Song, Y. Ota, W. Qiao, A. Tanaka and I. Mochida, *Carbon*, 2004, **42**, 1723-1729.
24. M. Wu, Q. Zha, J. Qiu, Y. Guo, H. Shang and A. Yuan, *Carbon*, 2004, **42**, 205-210.
25. A.-N. A. El-Hendawy, *Applied Surface Science*, 2009, **255**, 3723-3730.
26. Y. Dong, H. Lin, Q. Jin, L. Li, D. Wang, D. Zhou and F. Qu, *J. Mater. Chem. A*, 2013, **1**, 7391.

27. H.-T. Shu, D. Li, A. A. Scala and Y. H. Ma, *Separation and Purification Technology*, 1997, **11**, 27-36.
28. M. Hofman and R. Pietrzak, *TheScientificWorldJournal*, 2012, **2012**, 297654.
29. V. Fierro, V. Torné-Fernández, D. Montané and A. Celzard, *Microporous and Mesoporous Materials*, 2008, **111**, 276-284.
30. G. Yang, H. Chen, H. Qin and Y. Feng, *Applied Surface Science*, 2014, **293**, 299-305.
31. C. Moreno-Castilla, *Carbon*, 2004, **42**, 83-94.
32. M. A. Fontecha-Camara, M. V. Lopez-Ramon, M. A. Alvarez-Merino and C. Moreno-Castilla, *Langmuir*, 2006, **22**, 9586-9590.
33. F. C. Wu, R. L. Tseng, S. C. Huang and R. S. Juang, *Chemical Engineering Journal*, 2009, **151**, 1-9.

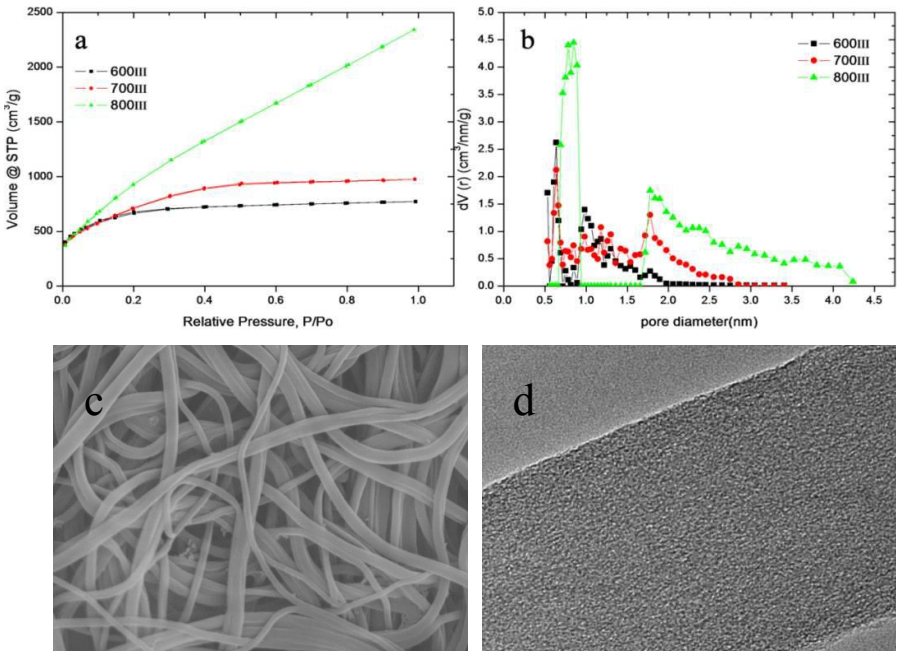

Activated carbon nanofibers fabricated through solution blowing and activation possessed a high special surface area and excellent adsorption capacity.